Single crystalline silicon dioxide films on Mo(1 1 2) ☆

T. Schroeder [a], A. Hammoudeh [b], M. Pykavy [a], N. Magg [a], M. Adelt [a],
M. Bäumer [a,*], H.-J. Freund [a]

[a] *Fritz-Haber-Institut der Max-Planck-Gesellschaft, Faradayweg 4-6, 14195 Berlin, Germany*
[b] *Department of Chemistry, Yarmouk University, P.O. Box 566, Irbid, Jordan*

Abstract

A preparation is reported which, for the first time, results in a thin, crystalline SiO_2 film on a Mo(1 1 2) single crystal. The procedure consists of repeated cycles of Si deposition and subsequent oxidation, followed by a final annealing procedure. LEED pictures of high contrast show a crystalline SiO_2 overlayer with a commensurate relationship to the Mo(1 1 2) substrate. Surface imperfections have been studied by SPA-LEED and a structure model, consistent with the appearance of antiphase domain boundaries as preferential disorder, is proposed. AES and XPS have been used to control film stoichiometry. A spatial dependence of the Si^{4+} core level shift with distance from the interface plane is observed and well explained by image charge interaction across the interface. Furthermore, the theoretically predicted insensitivity of the Si^{4+} core level shift with respect to the degree of crystallinity is experimentally verified for the first time. The wetting of the substrate by the film has been investigated by XPS and TDS. The results prove that the film covers the substrate completely. © 2001 Elsevier Science Ltd. All rights reserved.

Keywords: Crystalline SiO_2; Epitaxy; TDS; XPS; SPA-LEED; LEED; AES; Image charge; Tridymite; Metal–insulator interface

1. Introduction

In semiconductor industry, the properties of SiO_2 and the SiO_2/Si interface are essential for the performance of electronic devices. New generations of metal oxide semiconductor field effect transistors require a scaling down of the thickness of the insulating SiO_2 layer to less than 10 Å [1]. As one of the inherent problems in producing MOS gates in very large scale integrated circuits is reliability of the thin insulator layer, a complete understanding of the properties of thin SiO_2 layers in the vicinity of interfaces is imperative. Here, the SiO_2/Mo system can serve as a model system to clarify some of the key features of the SiO_2/Si interface. This approach offers the unique opportunity to study the influence of structure on silica thin film properties by changing the long-range order in the film from a nearly amorphous to a crystalline state [2].

2. Experimental

The film preparation starts with four cycles of Si deposition each followed by subsequent oxidation. Si is evaporated by electron bombardment of a Si rod keeping the crystal at 300 K. The subsequent oxidation step is carried out at 800 K in an atmosphere of 5×10^{-5} mbar O_2 (6 min). Spectra taken during film deposition have been recorded after each oxidation step and are denoted according to the corresponding cycle (1–4). After the SiO_2 film deposition, four annealing steps are applied to order the film. The crystal is heated in an atmosphere of 5×10^{-6} mbar O_2 for 20 min applying

---

1000 K during the first two and 1150 K during the last two annealing steps. Spectra taken during this preparation stage are denoted by the numbers 5–8 according to the respective annealing step.

3. Discussion

3.1. Crystallinity

Fig. 1 shows the result of our LEED study in terms of the clean Mo(1 1 2) surface (0), for reference, and the patterns obtained at the end of SiO_2 film deposition (4) and SiO_2 film annealing (8). The clean Mo(1 1 2) surface (0) exhibits a p(1×1) pattern, indicating that the surface preserves the trough and row structure with its rectangular unit mesh expected from the bulk (shown in Fig. 1) [3]. In the following, the spots at the position of the substrate spots will be referred to as fundamental spots. SiO_2 film deposition results in the appearance of faint and streaky superlattice spots in the centre of the rectangular substrate unit mesh which gain intensity with progress in film deposition. At the end of film deposition, the LEED pattern (4) consists of sharp fundamental and faint superlattice spots with a high background. Four annealing steps have been applied to order the film and the LEED pattern (8) shows the final result. The superlattice and fundamental spots appear to have similar intensities now and background is low, confirming the importance of the annealing steps to improve the crystallinity of the film. Film and substrate unit mesh are simply related and thus a commensurate growth of the SiO_2 film on the rectangular Mo(1 1 2) surface takes place. The film unit mesh has a $c(2×2)$ symmetry with respect to the substrate and the film unit cell length is derived to be 5.2 Å.

Taking a closer look, the LEED pattern reveals the surface imperfections which emerge during the growth of the SiO_2 film. In the final LEED pattern (Fig. 1, right), we observe a spot broadening of all the superlattice spots whereas all the fundamental spots remain sharp and isotropic. Note that the superlattice spots are broadened in both directions but anisotropically, resulting in a streaky, elliptical spot shape in the $\underline{a}_2^*$ direction. Such a behaviour is known from X-ray diffraction [4] and spot profile analysis (SPA)-LEED studies [5] and has been shown to arise from antiphase domain boundaries. As disorder in a certain direction produces streaks perpendicular to this direction, the strong broadening in the $\underline{a}_1^*$ direction indicates the existence of line defects running preferentially along the $\underline{a}_2$ direction. As the beams which will be broadened by the presence of antiphase domain boundaries depend on the way the domains are arranged with respect to each other [6], it is also possible to determine the displacement vector, connecting two antiphase domains. For

this purpose, it is helpful to make use of the structure model depicted in Fig. 1. It shows a top view of the Mo(1 1 2) surface with its trough and row structure (atoms in the upper layer: thick lines, atoms in the lower level: thin lines). The axis ratio of the rectangular surface mesh is such that a nearly hexagonal symmetry results on the surface. The corresponding unit mesh, which obviously triggers the growth of the crystalline SiO_2 film (see LEED pattern), is indicated in the figure with dotted lines. Due to this structure of the Mo(1 1 2) surface, six pseudo-equivalent three-fold hollow sites can be found around a given surface atom. Note, however, that these sites are not all equivalent, but that two sets of different type exist due to the corrugation of the Mo(1 1 2) surface. One type consists of two Mo atoms in the upper and one atom in the lower layer (A site), the other type of one atom in the upper and two atoms in the lower layer (B site).

Within this quasi-hexagonal network, there are now two possibilities to create domain boundaries, which run along the $\underline{a}_2$ direction. These are drawn with solid lines and are denoted by "type 1" and "type 2" in the figure. They differ with respect to the displacement vector connecting the domain in the lower part of the picture and the two domains in the upper part. Whereas the boundary of type 1 just requires a displacement in the $\underline{a}_1$ direction, boundaries of type 2 require a displacement vector of $(1/2\ \underline{a}_1 + 1/2\ \underline{a}_2)$. In the first case, alternating rows of broadened (or split) superstructure beams and sharp fundamental beams are expected along the $\underline{a}_1^*$ direction. In the second case, rows of broadened beams should run diagonally through the LEED pattern, i.e. both, fundamental and superstructure spots, are affected. Since the first situation is encountered in the present case, boundaries of type 2 can be ruled out.

In order to understand the preference of type 1 boundaries, we refer to the structure model again. Two assumptions are necessary to arrange the atoms of the SiO_2 overlayer on the Mo substrate: (a) the SiO_2/Mo interface consists of oxygen atoms chemisorbed on Mo(1 1 2); (b) the majority of oxygen atoms are located in the quasi-three-fold hollow sites denoted A of the Mo support. While the first point is confirmed by the XPS results discussed later, the second point can be justified by the general tendency of oxygen to bind to those highest coordination sites on transition metal surfaces on which also an additional metal layer would have grown [7]. If now the third oxygen atom completing the triangular face of the tetrahedral SiO_4 unit that is attached to the Mo(1 1 2) is situated in the less favoured B site (Φ), the Si atoms closest to the Mo substrate are found to form a regular $c(2×2)$ structure. The structure model we have developed so far turns out to be the (0 0 0 1) face of β-tridymite. As the lattice parameters of this modification fit to the model within 4%, this seems to be a reasonable assignment [8].
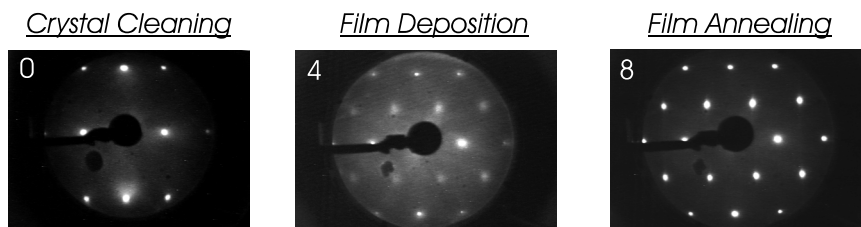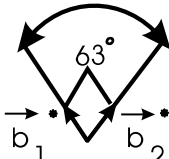
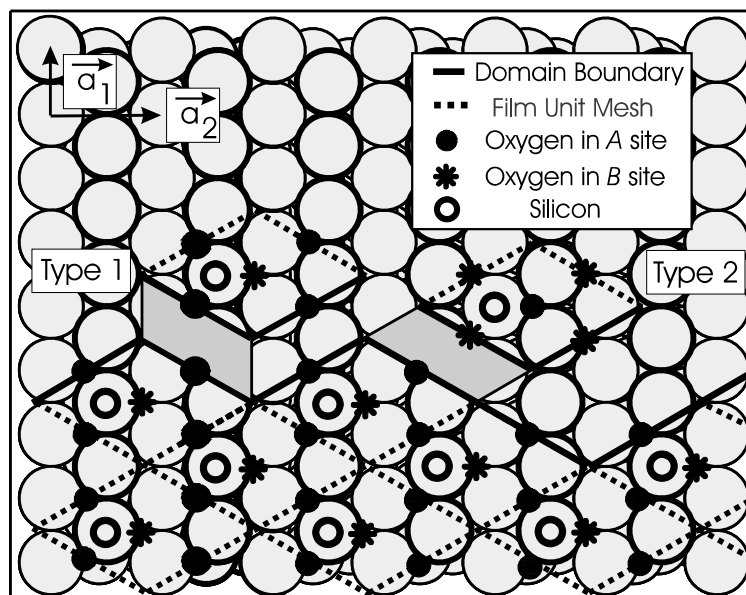Fig. 1. Reciprocal space: LEED pictures at $E = 56$ eV of clean Mo(1 1 2) (0), after SiO_2 film deposition (4) and after SiO_2 film annealing (8) with sketches of the respective unit meshes and their epitaxial relationship; real space: β-tridymite (0 0 0 1) as structure model for $SiO_2/Mo(1\,1\,2)$ with antiphase domain boundary running along the $\underline{\mathbf{a}_2}$ direction.

The preference of type 1 boundaries can now easily be explained by the oxygen adsorption behaviour. Only for type 1 boundaries, the preferred A site can be kept throughout all domains, while a type 2 boundary is connected with a change of sites. Note that the same arguments hold for the construction of antiphase domain boundaries along the $\underline{\mathbf{a}_1}$ direction (not discussed here) which are also present in the SiO_2 film.

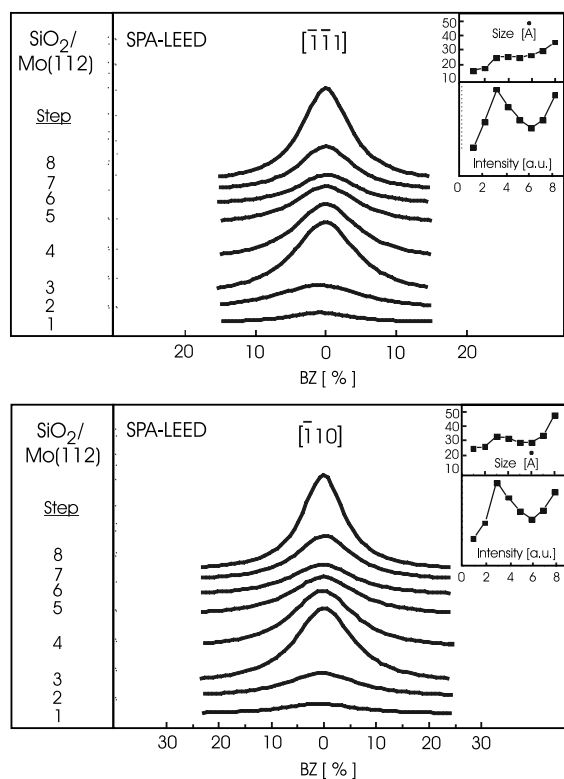In order to get quantitative information on the defect structure, a SPA-LEED study has been carried out,

Fig. 2. SPA-LEED study at $E = 56$ eV of the superlattice spot $(-1/2; -3/2)$ during film deposition (1–6) and film annealing (7,8) in $[-1 -1 1]$ direction (top) and $[-1 1 0]$ direction (bottom). Upper inset shows mean domains size D, lower inset the spot intensity.

which is presented in Fig. 2. The two plots show profiles of the $(-1/2, -3/2)$ superstructure spot along the $\mathbf{a}_1^* = [-1,-1,1]$ and the $\mathbf{a}_2^* = [-1,1,0]$ direction taken after each preparation cycle at an electron energy of 56 eV. In order to follow the developments with progress in film growth in more detail, the preparation procedure has been changed for this experiment. The film deposition was carried out in six cycles here (1–6). Film annealing was performed at 1100 K (7) and 1200 K (8).

Using mathematical formalisms as are described in the literature, the mean lateral extensions of the anti-phase domains can be calculated from the spot profiles [4]. For the evaluation of the present data, a constant probability for a displacement fault (i.e. the generation of a domain boundary) was assumed since this gives rise to lorenzian spot profiles as are observed in our case (see Fig. 2). The results can be found in the insets of Fig. 2. Accordingly, the extensions of the domains are different along the two high symmetry directions considered here. The average domain length along $[-1 1 0]$ is always larger as compared to $[-1 -1 1]$ resulting in final values of 50 and 35 Å, respectively. Furthermore, it is worth

noting that the intensity of the superlattice spot goes through a maximum after applying the third deposition cycle. Although not discussed here (see Ref. [2]), the first film monolayer starts to be completed here and the attenuation of the intensity of the superlattice spot (later on recovered by the annealing procedure) may be due to a modified Stranski–Krastanov growth mode: after formation of a first well-ordered, substrate stabilized SiO_2 layer (1–3), islands with reduced long-range order begin to grow on the next level (3–6) which require the high temperature treatment of the annealing procedure (7,8) to become crystalline.

3.2. Stoichiometry

3.2.1. Auger electron spectroscopy

Fig. 3 shows differentiated AE spectra taken for the clean Mo(1 1 2) substrate (a), after depositing Si (b) and at the end of film preparation (c). The most intense peak in the AE spectrum of the Mo(1 1 2) surface is the $M_{4,5}NV$ transition at 187 eV [9]. The attenuation of this substrate peak is used to derive an estimate of film thickness. All well-ordered SiO_2 films prepared in this study range in film thickness between 5 and 8 Å.

The deposition of Si leads to a strong feature at 92 eV which can be assigned to the $L_{2,3}VV$ transition of elemental Si [10,11]. Due to the high reactivity of Si with respect to oxygen, a small signal is always visible at 84 eV, i.e. close to the position expected for SiO ($L_{2,3}VV$) [10,11]. At the end of film preparation, i.e. after film annealing, the Si $L_{2,3}VV$ line shape is split into a main peak at 78 eV (Si $L_{2,3}V_1V_1$) and a satellite at 64 eV (Si $L_{2,3}V_2V_1$). They reflect the two maxima in the density of states of the SiO_2 valence band, originating from the
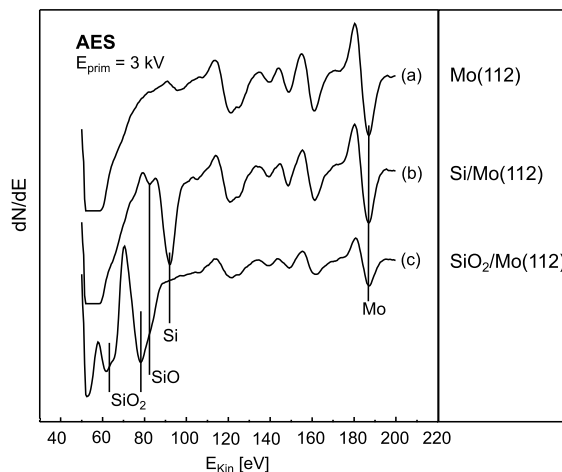

Fig. 3. AE spectra at different stages of film deposition: (a) clean Mo(1 1 2), (b) Si deposition on clean Mo(1 1 2) and (c) SiO_2 film on Mo(1 1 2).

participation of O_{2s} and O_{2p} orbitals. This spectrum is in line with reference spectra of silica samples, thus providing first evidence for the successful preparation of a stoichiometric SiO_2 film on the Mo substrate [10,11].

3.2.2. X-ray photoelectron spectroscopy

XPS has the advantage that, via the Si_{2p} core level shift, the different Si oxidation states can be resolved [12]. In Fig. 4, various Si_{2p} (left panel) and O_{1s} photoelectron spectra (right panel) of SiO_2 acquired during SiO_2 film deposition (1–4) and SiO_2 film annealing (6 and 8) are presented. The upper inset shows the development of position, the lower inset the evolution of intensity. Note that the position of the elemental Si_{2p} photoelectron line on Mo(1 1 2) is found at 99.3 eV (not shown here).

During SiO_2 film deposition (1–4), the intensity of the Si_{2p} photoelectron line scales linearly with the deposition cycles applied and decreases slightly ($\sim$15%) after film annealing (6 and 8). Such a Si loss can be the consequence of SiO_2 evaporation from rough surface regions having a higher vapour pressure [13] or desorption of volatile SiO [14].

First of all, the data from the Si_{2p} photoelectron line reveal that the growth of the SiO_2 film on Mo(1 1 2) is highly stoichiometric and differs from the SiO_2/Si interface by the absence of the Si suboxides, found in the transition region to adjust the density mismatch between the SiO_2 and Si lattice [12,15]. A further, most interesting point concerns the chemical shift of the Si^{4+} core level with progress in film preparation. During SiO_2 film deposition (1–4), a spatial dependence of the Si^{4+} core level shift with film thickness is observed (chemical shift increasing from 3.1 eV after the first to 3.6 eV after the fourth deposition cycle). Note that this Si^{4+} core level shift merely depends on film thickness, but not on film order: SiO_2 film annealing (6,8) results in a slight decrease of the FWHM from 1.8 to 1.7 eV, but no change in the position of the Si_{2p} signal is observed. The spatial dependence of the Si^{4+} core level shift with film thickness is well known from the SiO_2/Si interface [12,16] and an explanation based on the idea of image charge interaction across the interface has been proposed in that case [16]. This seems to be a reasonable interpretation also in the present case since other reasons, such as charging effects [17], can be excluded due to the advantageous situation of studying the thin film on a metallic substrate. Structural aspects, as proposed by Grunthaner et al. [18], seem unlikely as well, because we observe for the first time the theoretically predicted insensitivity of the Si^{4+} core level shift to the degree of crystallinity in the film [19].

An extra-atomic screening effect, for example due to the vicinity of a metallic interface, always reduces the core-level binding energy (BE) for the adsorbed atom compared to the free atom value [20]. Therefore, we estimate the effect of image charge interaction on the energy of the core hole in the growing SiO_2 film by applying a classical, dielectrical screening model. In Fig. 5, the Mo/SiO_2/vacuum system is described by three perfectly homogeneous media 1 (Mo), 2 (SiO_2) and 3 (vacuum) with the respective permittivities $\varepsilon_1 = +\infty$, $\varepsilon_2 = 2.1$ and $\varepsilon_3 = 1$ [16]. The core hole in medium 2 is represented by a point charge q located at a distance $(-a)$ from the left and at a distance b from the right boundary, with d being the distance between the two boundaries, i.e. the SiO_2 film thickness. In order to find the electrostatic potential V and the energy at the position of the point charge q in medium 2, we must solve the Laplace equation in cylindrical coordinates by making use of the boundary conditions at the left and right interface [21,22]. The resulting formula is given by

$$E_2 = \frac{q^2}{16\pi\varepsilon_2} \sum_{n=0}^{\infty} (k_1 k_2)^n \left[\frac{k_1}{a+nd} + \frac{k_2}{b+nd} + \frac{2k_1 k_2}{a+b+nd} \right] \tag{1}$$

adding the contributions of an infinite series of reflected images, mirrored at the two interfaces. The first set of reflected images is shown in Fig. 5 and the reflection coefficients k_1 and k_2 are defined by

$$k_1 = \frac{\varepsilon_2 - \varepsilon_1}{\varepsilon_2 + \varepsilon_1}; \quad k_2 = \frac{\varepsilon_2 - \varepsilon_3}{\varepsilon_2 + \varepsilon_3} \tag{2}$$

Eq. (1) can now be used to calculate the stabilization energy of a core hole situated in a distance a from the metallic interface. Note that, for $a \to 0$, the energy equation diverges and therefore we limit the calculation to a physical reasonable distance a of about 1.6 Å (O–Si bond length). It is noteworthy that the found correction energies are higher for the Mo/SiO_2 system (b,c,d) as for the Si/SiO_2 interface (a) due to the higher
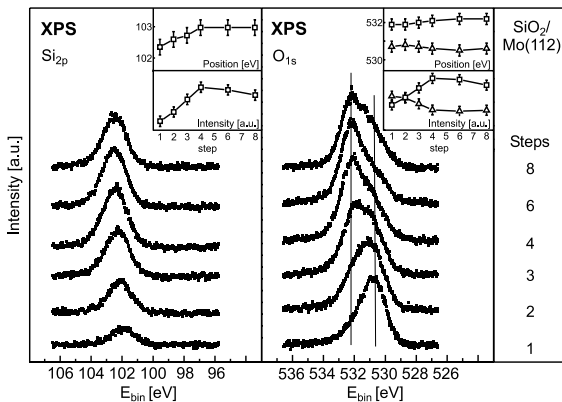

Fig. 4. Si_{2p} (left) and O_{1s} (right) photoelectron spectra recorded during SiO_2 film deposition (1–4) and SiO_2 film annealing (6,8). Upper inset shows the position, lower inset the intensity of the lines ($\square$: Si_{2p} and O_{1s} signal from SiO_2; $\triangle$: O_{1s} signal from oxygen chemisorbed on Mo(1 1 2)).
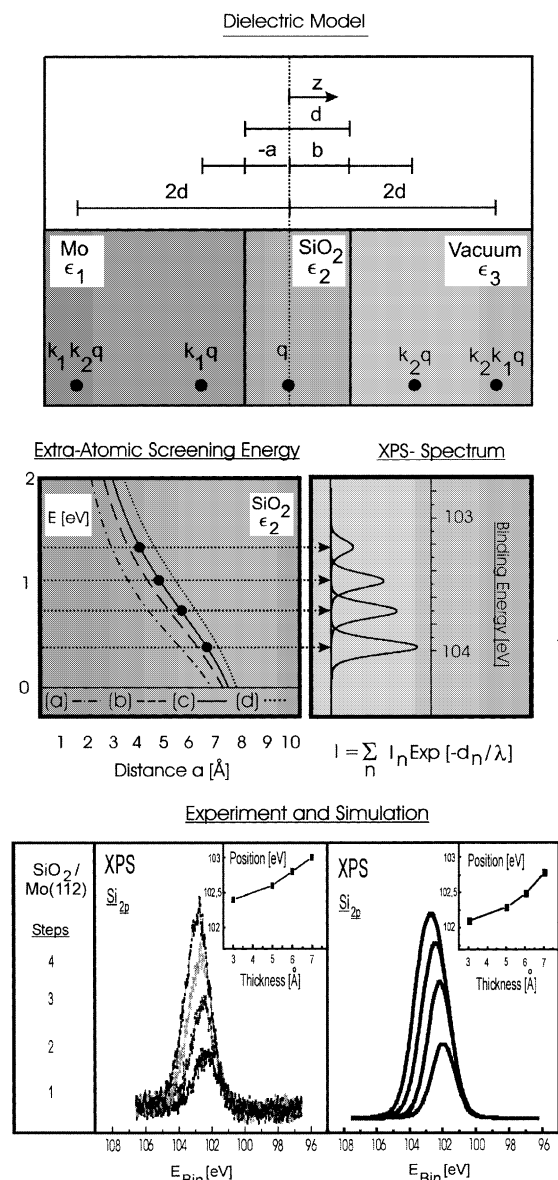
Dielectric Model

Extra-Atomic Screening Energy   XPS- Spectrum

$I = \sum_n I_n \exp[-d_n/\lambda]$

Experiment and Simulation

Fig. 5. Illustration of a dielectric model based on the permittivities ε to treat the Mo/SiO$_2$/vacuum system which explains the spatial dependence of the extra-atomic screening energy with distance a from the interface for Si/SiO$_2$ (a) and Mo/SiO$_2$ (b,c,d); the resulting XP spectrum is the superposition of energetically shifted and attenuated signal contributions from different layers in the oxide. Experiment and Simulation compares the calculation with the measurement for growing film thickness d.

dielectric discontinuity in this system (see Fig. 5). Furthermore, the correction energies turn out to be very sensitive to the dielectric constant ε_2 of SiO$_2$ and increase for decreasing values of ε_2. Band bending effects in insulators next to metallic interfaces are well known for

SiO$_2$ and result in a decrease of the dielectric constant as compared to the bulk value [1]. To visualize this effect, we calculated the energy correction by using for SiO$_2$ the bulk value of $\varepsilon_2 = 2.1$ (c) as well as a 30% lower ($\varepsilon_2 = 1.8$ (d)) and a 30% higher ($\varepsilon_2 = 2.4$ (b)) permittivity. Finally, the change in BE as function of position in the oxide is calculated by subtracting the spatially dependent image force interaction energy from the reference BE shift of 4.4 eV found for bulk SiO$_2$ [12,19]. Each of these BEs is then used as a position of a Gaussian like line shape which represents the signal contribution from the given oxide level. The line width is chosen to be similar to that measured experimentally (FWHM $\sim$1 eV). All these shifted Gaussians are then added taking the different intensities according to the inelastic electron mean free path in the oxide into account.

The result of our model calculation is compared in the lower part of Fig. 5 to the experiment. The plots clearly show that the resulting Si^{4+} photoelectron line from the Mo/SiO$_2$ system can indeed be regarded as a superposition of energetically shifted signal contributions from the different layers in the oxide. The effect of electrostatic screening succeeds to explain the magnitude of 0.5 eV of the observed spatial dependence of the Si^{4+} core level shift, but is inaccurate in predicting the absolute energy position which results $\sim$0.2 eV too low.

The O$_{1s}$ photoelectron line in Fig. 4 consists of two peaks, which can be assigned to oxygen chemisorbed at the interface to the Mo substrate (530.7 eV) [23] and to oxygen tetrahedrally coordinated to Si (532.2 eV) [18], respectively. The peak at 530.7 eV decreases strongly with SiO$_2$ film deposition (1–4), but a rest intensity remains also for the closed SiO$_2$ film (6,8). As already discussed in the structure model, we take this as evidence that the SiO$_2$ film is connected to the Mo(1 1 2) support by chemisorbed oxygen atoms to the Mo(1 1 2) support. The O$_{1s}$ peak at 532.2 eV scales directly with the Si intensity, resulting in a Si:O ratio of $\approx$2. The energy separation between O$_{1s}$ and Si$_{2p}$ signal is found to be 429 $\pm$ 0.4 eV, which is further indicative of SiO$_2$ [18].

3.3. Wetting behaviour

3.3.1. X-ray photoelectron spectroscopy

In order to study the influence of the film preparation on the Mo substrate, Mo$_{3d}$ spectra have been taken which are presented in Fig. 6. A first set of spectra has been recorded during the different stages of the film preparation and, for reference, a second set without depositing any Si. This allows to compare the behaviour of the Mo substrate under the preparation conditions with and without film growth.

In the first case, the Mo signal is attenuated during film deposition (left panel of Fig. 6, steps 2 and 4), but regains intensity ($\sim$15%) during film annealing (steps 6 and 8). This is consistent with the observed Si loss (see
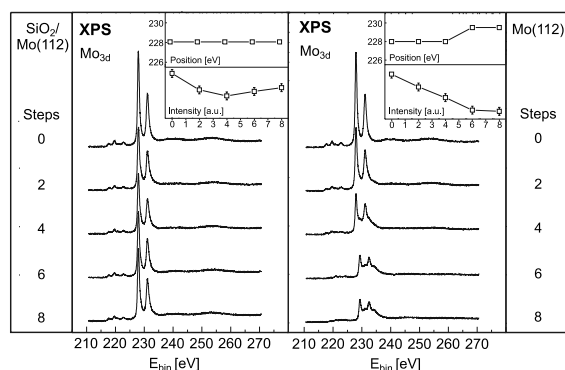
Fig. 6. Behaviour of the Mo_{3d} photoelectron line under film preparation conditions with a growing SiO_2 film (left panel) and without a growing SiO_2 film (right panel). Upper and lower insets show position and intensity of the line, respectively.

Fig. 4). It is noteworthy that no shift in the BE of the Mo_{3d} line can be detected throughout the whole procedure. Consequently, any oxidation of Mo or compound formation between Mo and Si can be excluded.

In the second case (see right panel of Fig. 6), a strong intensity attenuation of the Mo_{3d} line can be observed as well, if the film deposition conditions (2 and 4) are applied. During the annealing steps (6,8), the signal decreases further and finally reaches a saturation value. Although the shape and BE of the Mo_{3d} line do not alter during the first part of the preparation (2,4), appearance and position of the XP spectrum change drastically by applying the film annealing conditions (6,8). In fact, a fit procedure reveals that each spin–orbit component is now split into two components with an intensity ratio of $\approx$1:2. Without going into the details, such a spectrum is characteristic for MoO_2 [24]. Since uncovered substrate regions are obviously completely oxidized to MoO_2 under the film annealing conditions, the film coverage θ can be estimated by evaluating possible contributions of the MoO_2 spectrum to the spectrum of the SiO_2/$Mo(1 1 2)$ system. By a peak fit procedure, using the line positions and intensity distributions found for MoO_2 as input parameters, a coverage of at least 95% can be calculated [2].

3.3.2. Thermal desorption spectroscopy

In order to tackle the question of film coverage in more detail, a TDS experiment based on the idea of selective chemisorption has been carried out [2]. Deuterium (D_2) can be shown to adsorb on clean $Mo(1 1 2)$ [25] as well as on the oxygen-modified $Mo(1 1 2)$ [2] surfaces produced under conditions like those applied during the film preparation. As SiO_2 does not adsorb D_2 above 100 K [26], the adsorption sites on the substrate become more and more blocked as the film grows. Indeed, a complete suppression of the D_2 uptake is ob-

served after deposition and annealing of the SiO_2 film. Together with the experimental evidences reported above, this leads to the conclusion that a two-dimensional, continuous SiO_2 film is formed on the $Mo(1 1 2)$ support.

4. Conclusion and outlook

The growth of SiO_2 on a $Mo(1 1 2)$ single crystal results in a thin and well-ordered oxide film which is stoichiometric and continuous in nature. This system proves to be a helpful model to study the properties of thin SiO_2 layers in the vicinity of interfaces, including the influence of structural aspects. As a first example, the spatial dependence of the Si^{4+} core level shift with film thickness, known from the SiO_2/Si interface and discussed controversially [12,16], has been studied. For the first time, the theoretically predicted insensitivity of the Si^{4+} core level shift with respect to the degree of crystallinity in the film has been observed [19]. This result favours an explanation of the observed shift as being related to the dielectric discontinuity across the interface and is supported by an image charge interaction calculation.

For further experimental and theoretical studies, solving the crystal structure of the well-ordered SiO_2 overlayer on $Mo(1 1 2)$ is highly desirable. Here, β-tridymite (0 0 0 1) is proposed as a structure model for the SiO_2/$Mo(1 1 2)$ system, but a dynamical LEED study is under way to elucidate this point.

References

[1] Muller DA, Sorsch T, Moccio S, Baumann FH, Evans-Lutterodt K, Timp G. Nature 1999;399:758.
[2] Schroeder T, Adelt M, Richter B, Naschitzki M, Bäumer M, Freund H-J. Surf Rev Lett 2000;7(1,2):7–14.
[3] Braun O, Medvedev V. Sov Phys Usp 1989;32:328.
[4] Wilson A. X-ray optics, 2nd ed., Methuen, London, 1962.
[5] Libuda J, Winkelmann F, Bäumer M, Freund H-J, Bertrams Th, Neddermeyer H, Mueller K. Surf Sci 1994;318:61.
[6] Park RL. In: G.A. Somorjai, editor. The structure and chemistry of solid surfaces. New York: Wiley; 1968 [chapter 28].
[7] Over H. Prog Surf Sci 1998;58:249.
[8] Wyckoff RG. Crystal structures, 2nd ed., vol. 1. New York: Wiley; 1963.
[9] Zhang C, Van Hove MA, Somorjai GA. Surf Sci 1984;149:326.
[10] Carriere B, Lang B. Surf Sci 1977;64:209.
[11] Carriere B, Deville JP. Surf Sci 1979;80:278.
[12] Hollinger G, Himpsel F. Appl Phys Lett 1984;44:93.
[13] Markov I. Crystal growth for beginners. Singapore: World Scientific; 1995.
[14] Walkup R, Raider S. Appl Phys Lett 1988;53:888.
[15] Lu Z, Graham M, Jiang D, Tan K. Appl Phys Lett 1993;63:2941.

[16] Browning R, Sobolewski M, Helms C. Phys Rev B 1988;38:13407.

[17] Tao Y, Lu Z, Graham M, Tay S. J Vac Sci Technol B 1994;12:2500.

[18] Grunthaner FJ, Grunthaner PJ, Vasquez R, Lewis B, Maserjian J, Madhukar A. J Vac Sci Technol 1979;16: 1443.

[19] Pasquarello A, Hypertsen M, Car R. Phys Rev B 1996;53:10942.

[20] Egelhoff Jr WF. Surf Sci Rep 1987;6:253.

[21] Durand E. Electrostatique et Magnetostatique, Masson et Cie, 1953. p. 408.

[22] Kleefstra M, Herman GC. J Appl Phys 1980;51:4923.

[23] He J-W, Xu X, Corneille J, Goodman D. Surf Sci 1992;279:119.

[24] Brox B, Olefjord I. Surf Interf Anal 1988;13:3.

[25] Lopinski G, Prybyla J, Estrup P. Surf Sci 1993;296:9.

[26] Ko C, Gorte R. Surf Sci 1985;155:296.